Energy 250 (2022) 123729

Contents lists available at ScienceDirect

Energy

journal homepage: www.elsevier.com/locate/energy

Ultra-stable silica/exfoliated graphite encapsulated n-hexacosane phase change nanocomposite: A promising material for thermal energy storage applications

Sakshum Khanna [a], Sagar Paneliya [a], Parth Prajapati [b], Indrajit Mukhopadhyay [a], Hussam Jouhara [c, d, *]

[a] Department of Solar Energy, Pandit Deendayal Energy University, Gandhinagar 382421 Gujarat, India
[b] Department of Mechanical Engineering, Pandit Deendayal Energy University, Gandhinagar 382421 Gujarat, India
[c] Heat Pipe and Thermal Management Research Group, College of Engineering, Design and Physical Sciences, Brunel University London, UB8 3PH, UK
[d] Vytautas Magnus University, Studentu Str. 11, LT-53362 Akademija, Kaunas Distr., Lithuania

ARTICLE INFO

Article history:
Received 19 November 2021
Received in revised form
5 March 2022
Accepted 11 March 2022
Available online 19 March 2022

Keywords:
Phase change material
n-hexacosane
Nanocomposite
Thermal stability

ABSTRACT

In the current work, we demonstrate a simple, versatile, and scalable approach to synthesized silica encapsulated phase-change material (n-hexacosane) loaded between exfoliated-graphite nanosheets (ESPCM) by a chemical process (sol-gel and hydrothermal technique), exhibiting ultra-high thermal stability. The morphological, structural, and chemical properties of synthesized nanocomposite materials were investigated, and the results revealed that the PCM encapsulated within the silica shell was of diameters 120–220 nm and loaded in porous dendritic structures without any chemical reactions in phase change material. Further, the thermophysical properties such as latent heat, thermal conductivity, and stability of synthesized nanocomposites (ESPCM) were investigated by differential scanning calorimetry (DSC) and thermo-gravimetric analysis (TGA). During melting and solidification cycles, a solid-liquid phase transition of ESPCM nanocomposite was observed at 57.9 °C and 48.1 °C with a latent heat of 126.7 J/g and 117.6 J/g respectively. The ESPCM composites exhibited high thermal conductivity (15.74 W/m K) and ultra-high stability against thermal degradation after 300 thermal cycles. Subsequently, COMSOL simulations were carried out to investigate the thermal performance (heat flow with respect to time) of ESPCM, where, on increasing the EG concentration in the nanocomposite, an enhanced heat flow process was observed.

1. Introduction

In recent years, energy storage systems has drawn lot of attention for balancing the increase in energy demand [1–4]. Thermal energy storage systems are mainly classified as sensible heat storage and latent heat storage systems. Among storage systems, latent heat storage has an edge over sensible heat storage system as it offers high energy storage, low cost, minor chemical inertness or super-cooling, and low vapor pressure [5–11]. Organic phase change materials (OPCM) like n-hexacosane, fatty acids and polyethylene glycol have shown excellent properties, which make them a potential material for various applications such as solar heating systems, building materials and waste heat recovery system [12–14]. However, the major drawbacks associated with such OPCM are the low thermal conductivity, leakage problems and instability, which lower the overall performance of the thermal storage system. Until now, various measures have been taken to overcome the aforementioned problems. Some researchers have addressed the leakage issue and improved the stability of OPCM by microencapsulating the OPCM (as core) with various polymers as shell. The major disadvantage of such microencapsulation is the poor thermal conductivity of the core-shell or composite OPCM material [15–18]. Introducing thermally conductive additives to these encapsulating OPCM has also proved to be an effective way to address the thermal conductivity issue [19–23]. Among various thermal conductive additives, carbon-based nanomaterials like

* Corresponding author. Heat Pipe and Thermal Management Research Group, College of Engineering, Design and Physical Sciences, Brunel University London, UB8 3PH, UK
E-mail addresses: parth.prajapati@sot.pdpu.ac.in (P. Prajapati), indrajit.m@sse.pdpu.ac.in (I. Mukhopadhyay), Hussam.Jouhara@brunel.ac.uk (H. Jouhara).

https://doi.org/10.1016/j.energy.2022.123729

graphene, carbon nanotube, carbon fibre dots and exfoliated graphite have been used, which provide high thermal conductivity with stability and low density [24]. Exfoliated graphite (EG) is a highly porous material with a unique dendritic structure having low density and chemical activity, and high thermal conductivity. Due to its unique structure, it provides better supporting characteristics as compared to other carbon-based fillers. The addition of a suitable content of exfoliated graphite into encapsulated OPCM enhances the overall thermal conductivity and prevents leakages as it forms an ultra-shape-stabilized composite during the melting and solidification process. This unique feature makes exfoliated graphite a potential material for thermal applications. In 2007, Karaipekli et al. investigated the thermal conductivity and effect of various contents of EG in stearic acid (SA)/expanded graphite composites [25]. The results revealed that the thermal conductivity of the composite increased linearly with the increase of EG content. Similarly, Fang et al. [26] fabricated SA/EG PCMs with different EG mass loadings. The results indicated that when the EG mass content was nearly 17%, the corresponding phase-change latent heats were 155.5 kJ/kg. An increase in thermal conductivity was observed which was nearly 10 times that of pure SA.

Later in 2016, Xu et al. [24] fabricated d-Mannitol/expanded graphite (EG) composite PCM for solar thermal energy storage applications. The results showed that the EG prepared by the microwave synthesis method exhibited the maximum sorption capacity of 85 wt% for d-Mannitol. Also, an enhancement in the overall heat transfer process was observed during the charging/discharging process in the PCM composite due to high thermal conductivity. The mass fraction of EG and density of the composite PCM also affected the total heat storage duration. Similarly, Zhang et al. [27] and Yang et al. [28] fabricated capric-palmitic-stearic acid ternary eutectic mixture/expanded graphite (CA–PA–SA/EG) and myristic-palmitic-stearic acid/expanded graphite composite PCMs, respectively. The results showed an enhancement in the thermal conductivity of the composite on increasing the EG quality content (~10%).

In 2017, Weng et al. [29] developed a latent heat thermal energy storage system using fatty acids along with expanded graphite. The system showed promising results with increment in the encapsulation ratio, but lack of stability and leakage of the PCM diminished the overall energy storage capacity. Similarly, Hu et al. [30] synthesized palmitic acid/EG (PA/EG) composite PCMs with an EG mass fraction of 1%, 3%, 5%, and 8%. The result revealed that PA/EG composite consisting of numerous pores in expanded graphite nanosheet has the phase-change temperature near to PA. D. Zhou et *al.* [31] prepared Myristic acid/expanded graphite (MA/EG) composite phase-change material (CPCM) by absorbing PCM liquid between the EG nanosheet as a supporting material. The result showed that the latent heats during the melting and freezing process were 189.5 and 187.8 J/g, respectively. The MA/EG composite showed good thermal stability even after several heat-cycled accelerations. The addition of EG resulted in enhanced thermal conductivity as compared to pure MA. Recently, D.G. Atinafu et *al.* synthesized *a* biochar-integrated multiwalled carbon nanotube and used as a supporting material for a phase change material (n-dodecane). The phase change material introduced into pristine biochar and biochar-CNT revealed a heating enthalpy of 127.3 J/g and 152.3 J/g, respectively. The composite PCMs revealed high chemical compatibility and thermal stabilities [32]. These results indicate that the carbon nanomaterials can be used as a supporting material to enhance the thermal conductivity of the encapsulated OPCM materials for low-temperature thermal-energy-storage systems.

With reference to the exhaustive literature cited, the state of the art of the current work is to address the problems of leakage, low stability and the low thermal conductivity of the phase change material. Herein we present a simple, versatile and scalable chemical process to fabricate an ultra-stable nanocomposite consisting of n-hexacosane encapsulated silica (SPCM) as active material and exfoliated graphite (EG) as porous supporting material. The physical and chemical properties of ESPCM were characterized by scanning electron microscopy (SEM), transmission electron microscopy (TEM), and Fourier transformation infrared spectroscopy (FTIR). The effect of porosity, leakage of the composite material, phase transition temperature, latent heat, thermal decomposition temperature, and thermal or electrical conductivity were investigated using differential scanning calorimetry (DSC), thermogravimetric analysis (TGA), and infrared thermography. The as-prepared ESPCM composites can be used for thermal energy-storage systems that can store solar heat using daylight and release heat at night and they can be widely used in applications of energy storage.

2. Experimental section

2.1. Materials and method

Natural flake graphite (NG) of average flake size ~200 nm (99 wt %), nitric acid (70 wt %), Tetraethyl orthosilicate (TEOS), Absolute Ethyl alcohol (EtOH, C_2H_5OH, 99.9%, V/v), Cetyl Trimethyl Ammonium Bromide (CTAB), n-hexacosane, sulphuric acid (98 wt %), H_2O_2 (35 wt %) Ammonia (NH_3) and n-amyl alcohol of analytical grade purchased from Sigma Aldrich Inc were used without further purification. All the experiments were conducted using ultrapure water of resistivity 18.2 MΩ cm.

2.2. Preparation of n-hexacosane encapsulated within silica shell (SPCM)

The optimized silica nano-encapsulated phase change material (SPCM) was synthesized as per our previous reported work [33]. Initially, 2 g of n-hexacosane was mixed with 50 ml of C_2H_5OH alcohol in a round flask under continuous stirring at 70 °C. A change in the transparency of solution was observed and simultaneously a mixture consisting of CTAB, n-amyl alcohol and precursor TEOS of 1 ml was added into the flask. After rigorous stirring for 1 h, aqueous ammonia solution was added to the flask for precipitation [34] and left under continuous stirring for 6 h. The resulting composite was centrifuged at 6000 rpm for 30 min and washed with alcohol multiple times to remove the residue. Similarly, pure silica was prepared using the aforementioned sol-gel method to compare various properties with the nanocomposites.

2.3. Preparation of SPCM loaded exfoliated graphite nanosheet (ESPCM)

First, natural graphite was immersed in a 20 ml H_2O_2 solution, ultrasonicated for 15 min and the solution was kept for 20 min under ambient stirring. The pre-oxidized treated graphite was added to 25 ml acid solution containing sulphuric acid and nitric acid (4/1, v/v%) and placed in an ice bath for an hour. The resultant product was filtered and washed many times with deionized water to lower the acidic pH (5–6 pH). Second, the exfoliated graphite was dispersed in ethyl alcohol solution with SPCM and stirred for 45 min at 65 °C. Later, the solution was quickly placed and sealed in a 30 ml Teflon-lined autoclave at 80 °C for 60 min and cooled naturally. The resultant product was washed with DI water until the pH reached neutrality and left overnight for drying. Next, the dried sample was placed in an oven for 90 min at 70 °C to obtain various encapsulated SPCM loaded exfoliated graphite nanocomposite as

shown in Fig. 1. Similarly, pure exfoliated graphite was prepared using the above method to compare various morphological and structural properties of the supporting matrix with the nanocomposites.

Depending on the exfoliated graphite content (5 wt %, 10 wt % and 20 wt %) with encapsulated SPCM, various samples were synthesized and were labelled E1SPCM, E2SPCM, E3SPCM as shown in Table 1. Further, various ESPCM pellets were formed into cylindrical blocks using a hydraulic press (1 cm diameter and height) under the pressure of 50 kg/cm^2. Actual packing densities were calculated by the actual masses to volumes of the cylindrical blocks formed as shown in Table 1.

2.4. Instrumentation

In the current section, the specifications of the instruments used for the experimental investigation are described. Morphological and structural analysis was carried out to study the phase transition and stability of the synthesized nanocomposite.

2.4.1. Morphological and structural analysis

The surface analysis was carried out using a Field Emission-Scanning Electron Microscope (FESEM) (Zeiss Ultra 55) operated at 5 KeV and Transmission Electron Microscope (TEM) (JEOL 2100) operated at 200 KeV with a point-to-point resolution of 0.19 nm. The structural and chemical properties of as-prepared ESPCM samples were analyzed using Raman spectroscopy (Renishaw in via Raman microscope, laser of wavelength 532 nm), X-ray Diffraction (Panalytical, X'PertPRO, $\lambda = 1.54$ Å), and Fourier Transform Infrared Spectroscopy (FTIR, Malvern).

2.4.2. Thermal analysis

The phase transition temperature and latent heat of the ESPCM composite were measured using a differential scanning calorimeter (DSC) (PerkinElmer DSC 8000). Prior to measurement, the sample was weighed and sealed in an aluminium pan. Heat flow measurement was carried out with a heating rate of 2 °C/min under a constant stream of argon at a flow rate of 10 ml/min. The mass of the PCMs for each test was ~3.10 mg. Weight loss or Mass fraction analysis was carried out using a Thermogravimetric Analyzer (PerkinElmer TGA 4000) with a heating rate of 5 °C/min from room temperature to 600 °C. The average value from five replicated tests for each PCM was reported.

The thermal conductivity of various ESPCM samples was measured using the transient hot wire method as shown in Fig. S1 (Supplementary Information). The measurement is a sequential response of the wire temperature when current passes through its circuit. In the experiment, a Platinum (Pt) hot wire (diameter ~76.4 mm) was used as a heater and resistance thermometer with an insulating coating of Teflon [23]. The thermal conductivity is calculated by Fourier's law of heat transfer using:

$$k = \frac{Q}{4\pi L}\frac{dln(t)}{dt} \tag{1}$$

where 'L' shows the length of the wire, 't' is the total time, 'Q' is power supplied to the wire 'T″ is the temperature of the wire and 'k' represents the thermal conductivity. To ensure the accuracy of the measured thermal conductivity, each sample was tested 4 times at an interval of 15 min.

2.4.3. Software simulation

COMSOL Multiphysics offers simulation of various engineering phenomena in one environment and heat transfer study is one of them. To study heat transfer process within as prepared nanocomposite material, COMSOL enables a systematic simulation of melting and solidification cycle with respect to concentration of the carbonaceous material. Simulation for constant heat flux condition was carried out with the temperature of 70 °C on the boundary (one of the vertical wall of the sample). Upon application of heat flux, melting initiates and phase change material absorbs the energy and stores in the form of latent energy which can be utilised at later stage. For the simulation, conservation of energy, mass and momentum can be expresses as.

Mass conservation:

$$\frac{\partial \rho}{\partial t} + \frac{\partial(\rho u)}{\partial t} + \frac{\partial(\rho v)}{\partial t} = 0 \tag{2}$$

Momentum conservation:

$$\frac{\partial u}{\partial t} + u\frac{\partial u}{\partial x} + v\frac{\partial v}{\partial y} = \frac{1}{\rho_f}\left[-\frac{\partial p}{\partial x} + \mu_f\left(\frac{\partial^2 u}{\partial x^2} + \frac{\partial^2 u}{\partial y^2}\right)\right] \tag{3}$$

$$\frac{\partial v}{\partial t} + u\frac{\partial v}{\partial x} + v\frac{\partial v}{\partial y} = \frac{1}{\rho_f}\left[-\frac{\partial p}{\partial y} + \mu_f\left(\frac{\partial^2 v}{\partial x^2} + \frac{\partial^2 v}{\partial y^2}\right) + g(\rho\alpha_p)(T - T_m)\right] \tag{4}$$

Energy conservation:

$$\rho C_p\frac{\partial T}{\partial t} + \rho C_p u\cdot\nabla T + \nabla\cdot q = Q + Q_p + Q_{vd} \tag{5}$$

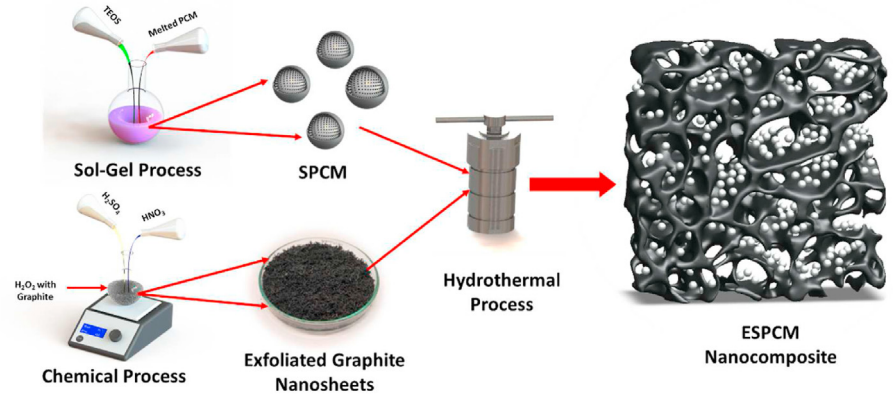

Fig. 1. Schematic showing the synthesis mechanism for ESPCM nanocomposites.

Table 1
Exfoliated graphite content in encapsulated SPCM composite.

S. No.	Material	EG Concentration (wt.%)	SPCM (wt.%)	Packing Density (kg/m^3)
1.	n-hexacosane	–	100	–
2.	E1SPCM	5	95	622.4
3.	E2SPCM	10	90	685.3
4.	E3SPCM	20	80	750.6

3. Result and discussions

3.1. Morphological analysis of nanocomposites

The morphology of synthesized exfoliated graphite (EG) nanosheets, EGPCM (exfoliated graphite with n-hexacosane), SPCM (n-hexacosane encapsulated within silica shell), and ESPCM were observed under FESEM and TEM as shown in Figs. 2 and 3. Fig. 2(a) shows the micrographs of exfoliated graphite (EG) synthesized using a chemical process as explained in Section 2.2. A highly porous dendritic structure with average length and width of ~400 ± 50 μm and ~80 ± 20 μm respectively was observed, and these abundant pores provide mechanical strength to loaded core-shell SPCMs nanocomposite as shown in Fig. S2 [33–35]. These nanoscale pore structures have a high surface area as compared to pristine graphite which was confirmed using Brunauer-Emmett-Teller (BET) analysis (~30 m^2/g) as shown in Fig. S3. Hence, this structure contributes high surface area and large volume and can be endowed with large adsorption capacity and support to SPCM nanocomposite. Fig. 2(b) shows the impregnation of n-hexacosane between the exfoliated graphite nanosheet, which confirms the absorption capacity of the base material (EG nanosheet). Fig. 2 (c) shows a smooth surface of a core-shell SPCM nanocomposite with enhanced homogeneity in size distribution, i.e., 180 ± 50 nm. Spherical morphology of silica shell was observed, indicating exceptional shell encapsulation and this prevents any leakage during the phase change process.

Fig. 2(d–f) shows the morphology of different ESPCM composites prior to melting and solidification cycles. Impregnation of core-shell SPCM was observed between the layers of graphitic nanosheets. The amount of impregnation of n-hexacosane and SPCM between the nano-sheets depends appreciably on the graphitic content and it also reduces the pores in the exfoliated structure. At lower graphitic content (*viz.* 5 wt% and 10 wt%), the loading of SPCM and its clusters were observed on the surface of the carbon material, indicating the presence of an excess of SPCM above the absorption capacity of the EG as shown in Fig. 2(d) and (e). Further increasing the graphitic content (20 wt %), high impregnation of SPCM was observed which filled all the pores of the graphitic material. The presence of remaining dendrite structures of EG enhances the thermal conductivity of the PCM composites (Fig. 2(f)).

Further, TEM imaging was also carried out to analyse the structure of ESPCM as shown in Fig. 3(a). Thin intercalated layers of graphite were also observed as shown in Fig. 3 (b), while an amorphous boundary of silica capsule over a high contrast PCM core was observed as shown in Fig. 3 (c). The TEM micrographs confirmed the encapsulation of PCM by an amorphous silica shell, which was impregnated between the graphitic nanosheets [33].

3.2. Structural and chemical analysis of nanocomposites

The crystallinity of n-hexacosane, exfoliated graphite, silica, SPCM, EGPCM and ESPCM composites was examined using X-ray diffraction spectroscopy, as shown in Fig. 4 (a). The characteristic peaks of n-hexacosane were observed at 2θ = 21.15° and 23.50°, indicating (110) and (200) crystal planes of n-hexacosane (JCPDS No. 40–1995), whereas a broad peak at 2θ = 23.55° in the silica sample shows the amorphous nature of silica formation [34–37]. XRD profile of SPCM shows both prominent peaks of n-hexacosane and the amorphous silica peak, while the higher-order peaks are suppressed. In addition, no extra diffraction peaks were observed other than EG, silica and n-hexacosane characteristic peaks at 2θ = 26.7° and 21.11°, 23.60° respectively, which indicates that the crystal structure (002) for exfoliated graphite and n-hexacosane remains unaltered, which is attributed to physical mixing and compression being used in the synthesis of the composites.

Fig. 4(b) shows the Raman measurement of n-hexacosane, exfoliated graphite, silica, SPCM, EGPCM and ESPCM composites. The peaks of pure phase change material i.e., ν = 1058 cm^{-1}, 1150 cm^{-1}, 1296 cm^{-1}, and 1460 cm^{-1} were observed and can be attributed to C–C (carbon-carbon) stretching and CH_2 and CH_3 deformation [33,38]. In addition, a D peak was observed for exfoliated graphite, which was more intense, and the I_D/I_G value for EG and G was observed to be 0.15 and 0.06, respectively, representing structural disordering in graphitic structure, supporting the XRD measurements (Fig. S4). Similarly, the characteristic peaks of silica at ν = 478 cm^{-1}, 802 cm^{-1} were observed, indicating R and D_1 line along with vibrational hydroxyl (OH^-) group with respect to Si [39–43]. Raman spectra of the ESPCM and SPCM show combined spectra of both exfoliated graphite sheet and silica with phase change material, supporting the XRD results. No new peaks were observed in ESPCM, this indicates that no chemical reaction took place between all the materials and the encapsulation of silica shell and nanosheets are through physical attachment or adsorption.

In order to determine the presence of organic and inorganic composition, FTIR spectroscopy was carried out for n-hexacosane, silica, EGPCM, SPCM and ESPCM composites as shown in Fig. 4(c). The vibrational peaks at 720 cm^{-1}, 1375 cm^{-1}, and 1464 cm^{-1} were attributed to CH_2 and C–H bonds present in n-hexacosane (PCM), while peaks at 1061 cm^{-1}, 801 cm^{-1}, 557 cm^{-1}, and 3001 cm^{-1}, 3502 cm^{-1} indicate the bending and stretching vibration of the silica's OH group. In addition, symmetrical and asymmetrical stretching vibration peaks of the C–H bond were observed at 2846 and 2910 cm^{-1}, respectively [42–46]. Post-loading of n-hexacosane encapsulated within silica shell into the exfoliated graphite by the hydrothermal process, no additional peak or any transformation in the spectrum were observed indicating no chemical reaction between materials and this demonstrates that the loading is through physical attachment.

3.3. Simulation of encapsulated n-hexacosane silica composite impregnated in exfoliated graphite nanosheets

COMSOL simulation was carried out to understand the behavior of heat diffusion within the nanocomposite material. Simulation helped to know the heat transfer rate during melting (absorption) and solidification (rejection) cycle wherein the nanocomposite strives to store and supply energy using its latent heat energy capacity [47].

Organic phase change material, n-hexacosane, is encapsulated in a silica shell to overcome the leakage problems but a low thermal conductivity of the composite still persists. The encapsulated core

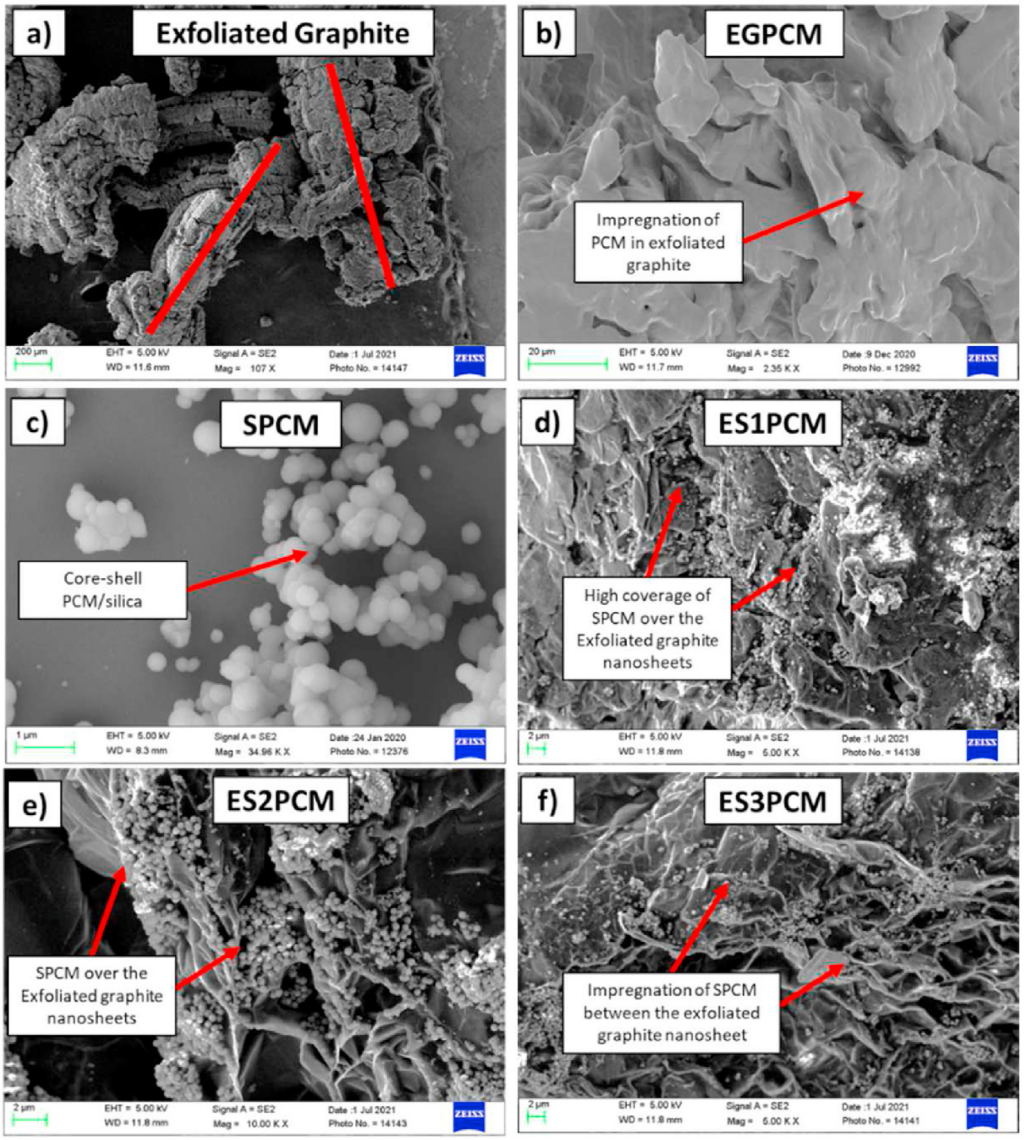

Fig. 2. FESEM micrograph showing (a) highly porous dendritic structure of EG, (b) EGPCM, (c) Nano-encapsulated PCM (SPCM). FESEM of ESPCM composites with various EG content (d) 5 wt % (e) 10 wt % and (f) 20 wt %.

material is loaded within the expanded graphite sheet which possesses high thermal conductivity and the meshed structure of the sample of nanocomposite. Schematic of the boundary conditions applied to the considered sample of nanocomposite is shown in Fig. S5. A heat source temperature of 70 °C is applied, higher than the solid-liquid transition temperature of the nanocomposite. The void between the expanded graphite sheets is filled up with encapsulated PCM which helps in the storage of energy at low temperatures, taking advantage of latent heat of the material.

The graphitic content was varied in the nanocomposite with encapsulated PCM and three samples with 5 wt% (E1SPCM), 10 wt% (E2SPCM) and 20 wt% (E3SPCM) were considered for simulation. The results of simulation were compared with pure n-hexacosane (PCM) in terms of time required to absorb and release the heat energy until complete melting and solidification respectively was observed. Figs. 5 and 6 show the temperature variation during the heat interaction for melting and solidification cycles, respectively.

With 5 wt % concentration, ~33% and ~22.5% reduction in time is observed as compared to pure n-hexacosane during melting and solidification cycles, which signifies that the presence of graphitic structures results in improved heat transfer rates. Similarly, for the samples with increased concentrations of 10 wt% and 20 wt%, the phase transition time reduced by 45.6% and 56.8% for melting and 40.2% and 52.3% for solidification respectively as compared to pure PCM. Figs. 5 and 6 show the temperature variation during the heat interaction for melting and solidification cycles. Table 2 shows the reduction in time for all the nanocomposite samples during simulation. Results of simulation were found to support the experimental results and the nanocomposite showed good characteristics in terms of enhanced heat transfer during the thermal cycles.

3.4. Absorption ratio of n-hexacosane in ESPCM composites

In general, the more the mass of organic phase change material in nanocomposites, the more the absorption of latent heat. In the case of ESPCM composites, EG plays the role of a supporting material to which PCM encapsulated within silica gets attached. During the melting process, the phase changes from a solid to a liquid

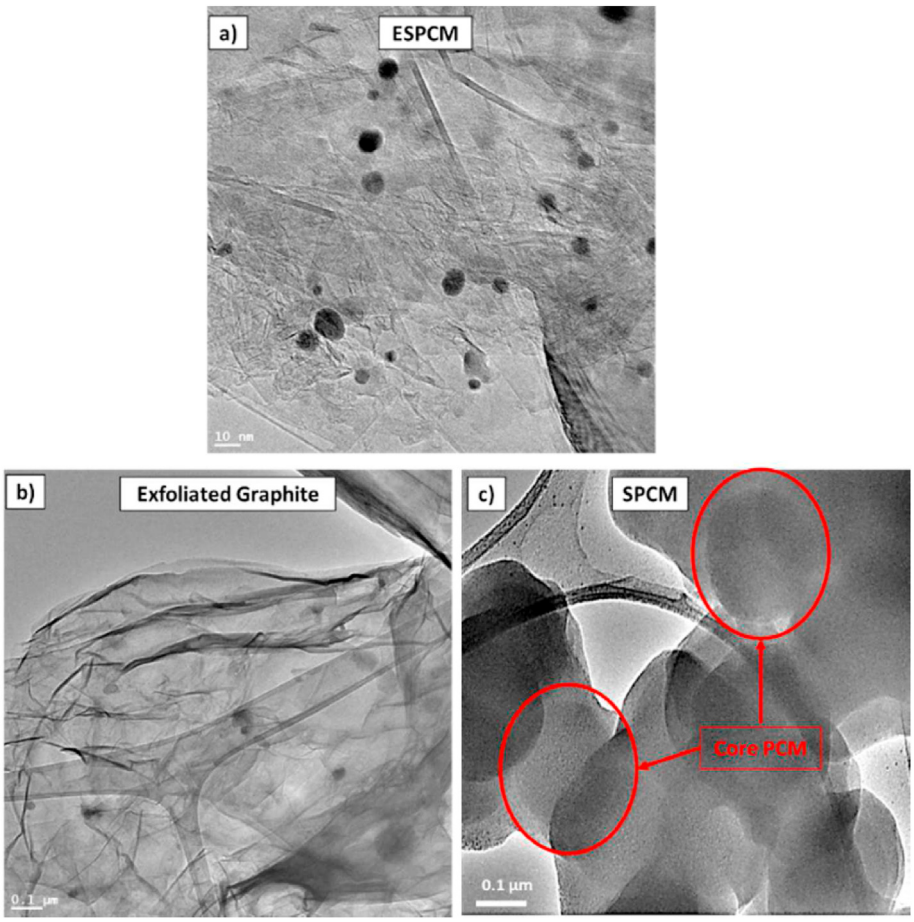

Fig. 3. TEM micrograph of (a) ESPCM, (b) EG and (c) SPCM.

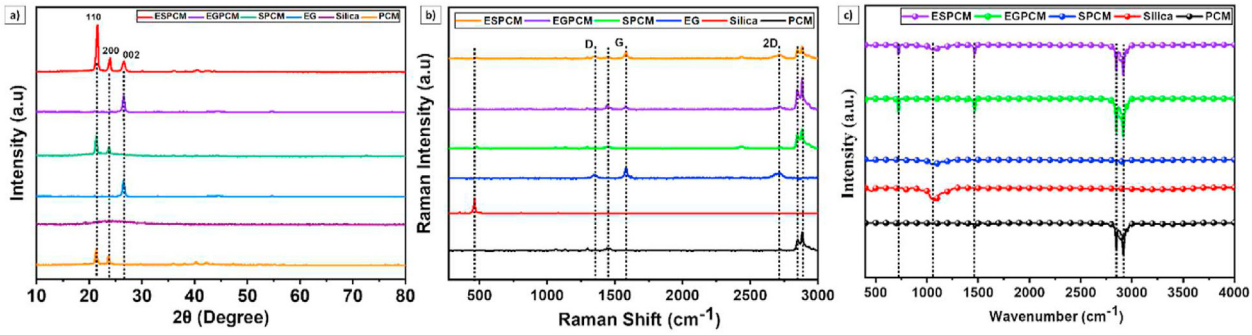

Fig. 4. (a) X-ray diffraction profiles and (b) Raman spectroscopy and (c) Fourier transform infrared spectroscopy of pure n-hexacosane and ESPCM composites (E1SPCM1, E2SPCM, and E3SPCM).

state; however, the physical attachment between the core material and shell material along with the capillary forces from the supporting matrix restrict the leakage of the PCM. Beyond the maximum encapsulation of the PCM, excess n-hexacosane tries to get attached to the surface of the composite, which leaks during the phase-change process. The variation in the EG mass fraction affects the phase-transition temperature and also improves the absorption on the matrix. Hence, the diffusion–exudation circle method was applied to confirm the mass rate of n-hexacosane in composite PCMs [32]. The test method diagram and process has been illustrated in Fig. S6. The different PCM composite samples containing EG contents (5 wt%, 10 wt% and 20 wt%), were processed to form composite pellets with a diameter of 10 mm and length 20 mm, which were placed over the centre of the filter-paper centre (as shown in Fig. S6) and the sample was kept on the heating plate at 70 °C. The degree of leakage of the phase change material in the sample was observed every hour outside the unit test area, as shown in Fig. 7. Depending upon the leakage, the results can be categorized as per the standard in stable, moderate stable or unstable samples as depicted in Table S6.

The stability of composite samples was calculated by estimating the leakage percentage (Ψ) and compared with the known range of exudations standard by calculating the average exudation-circle diameter to the sample diameter. The samples consisting of lower

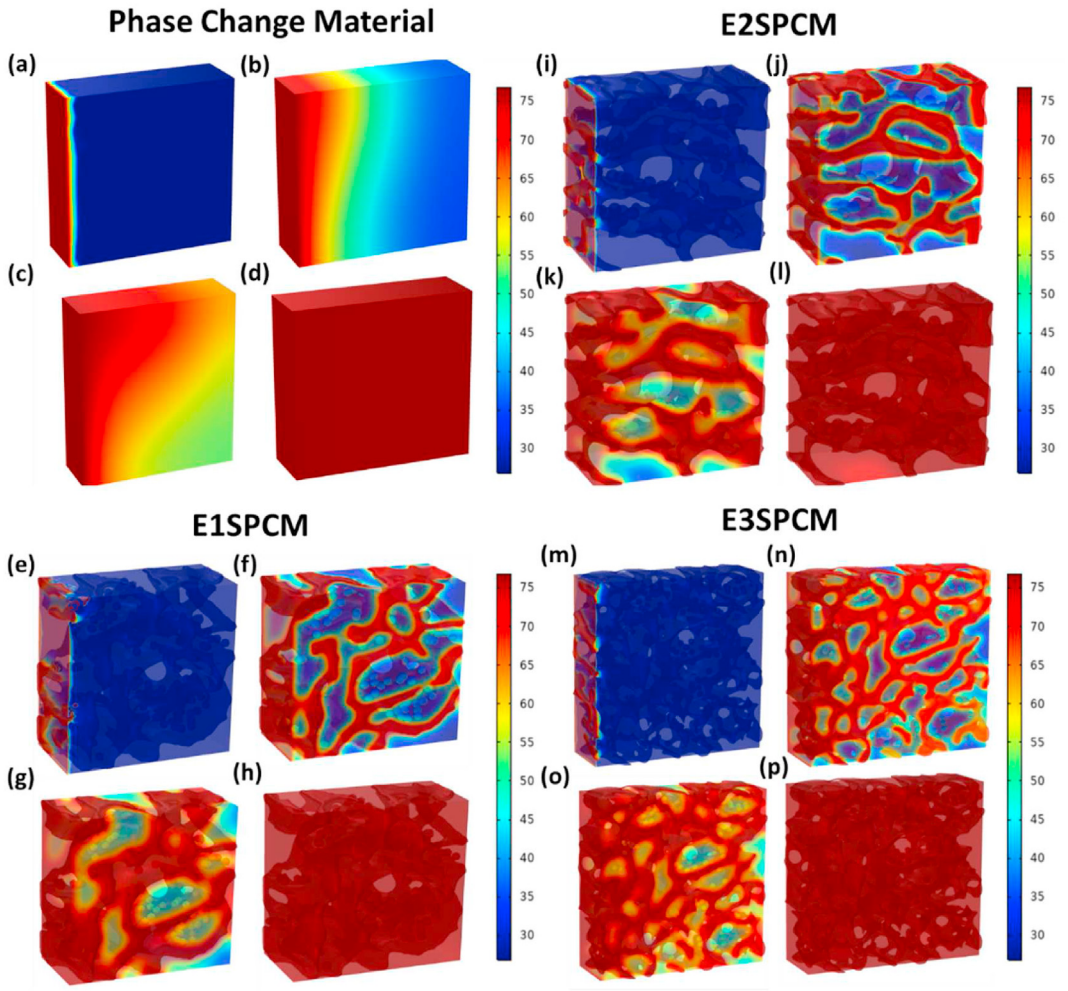

Fig. 5. COMSOL simulation of (a–d) n-hexacosane and ESPCM composite with various EG content (e–h) 5 wt% (i–l) 10 wt% and (m–p) 20 wt% respectively during melting process.

EG content resulted in leakage after 2 h, whereas no exudation or extremely minor exudation was found in higher EG content i.e., E3SPCM sample (EG ~ 20%). Hence, the E3SPCM was observed to be an ultra-stable composite, compared to other samples, and listed in Table 3.

3.5. Infrared thermal imaging

In order to study the temperature changes with respect to EG content, infrared (IR) thermal imaging was carried out for various ESPCM composites. The surface temperature distributions of the pure PCM and ESPCM composites were recorded, and the average surface temperatures were calculated as shown in Fig. 8. All the ESPCM composites showed quicker heat absorption and temperature regulation as compared to pure PCM at every moment due to the presence of expanded graphite, indicating the outstanding temperature and time regulating ability during the heating process. The average temperature E3SPCM attains after 480 s was 66.2 °C which was nearly 15% reduced as compared to pure n-hexacosane, indicating that on increasing the EG content in the composite, the overall heat absorption and transfer within the composite enhances. The silica encapsulated n-hexacosane impregnated inside the graphitic sheet adsorbed thermal energy during the charging process, while desorbed the energy during the discharging process. Therefore, the EGPCM composites can regulate temperatures depending on the phase change character of PCM material.

3.6. Thermal analysis of ESPCM composites

Differential scanning calorimetry is a thermal analysis technique which enables measurements of phase transitions and crystallizations of a given material. Samples of nanocomposite ESPCM were studied for the heat flow within the phase transition temperature range. From the results as shown in Fig. 9 (a), it was observed that a maximum heat flow of 184.6 J/g for pure n-hexacosane was obtained at 54.6 °C during the heating cycle (heat absorption). In other words, results revealed S–S and S-L transition occurred at 38.5 °C and 54.6 °C respectively. With inculcation of encapsulated n-hexacosane with silica shell impregnated into exfoliated graphite of 5 wt%, 10 wt% and 20 wt%, marginal reduction in heat flow is observed which is justified because of the reduction in latent heat capacity of n-hexacosane. Table 4 shows the melting and solidification temperature of n-hexacosane, E1SPCM, E2SPCM and E3SPCM along with their latent heats. The maximum heat flow peak of the nanocomposite shifts towards the right-hand side (with reference to the temperature axis) at 56.1 °C, 57.6 °C and 57.9 °C with the reduction in heat flow of 158.7 J/g, 142.8 J/g and 126.8 J/g respectively which indicates that the incorporation of the silica and expanded graphite lowers the overall latent heat storage capability.

A similar trend of heat flow is observed for the samples of

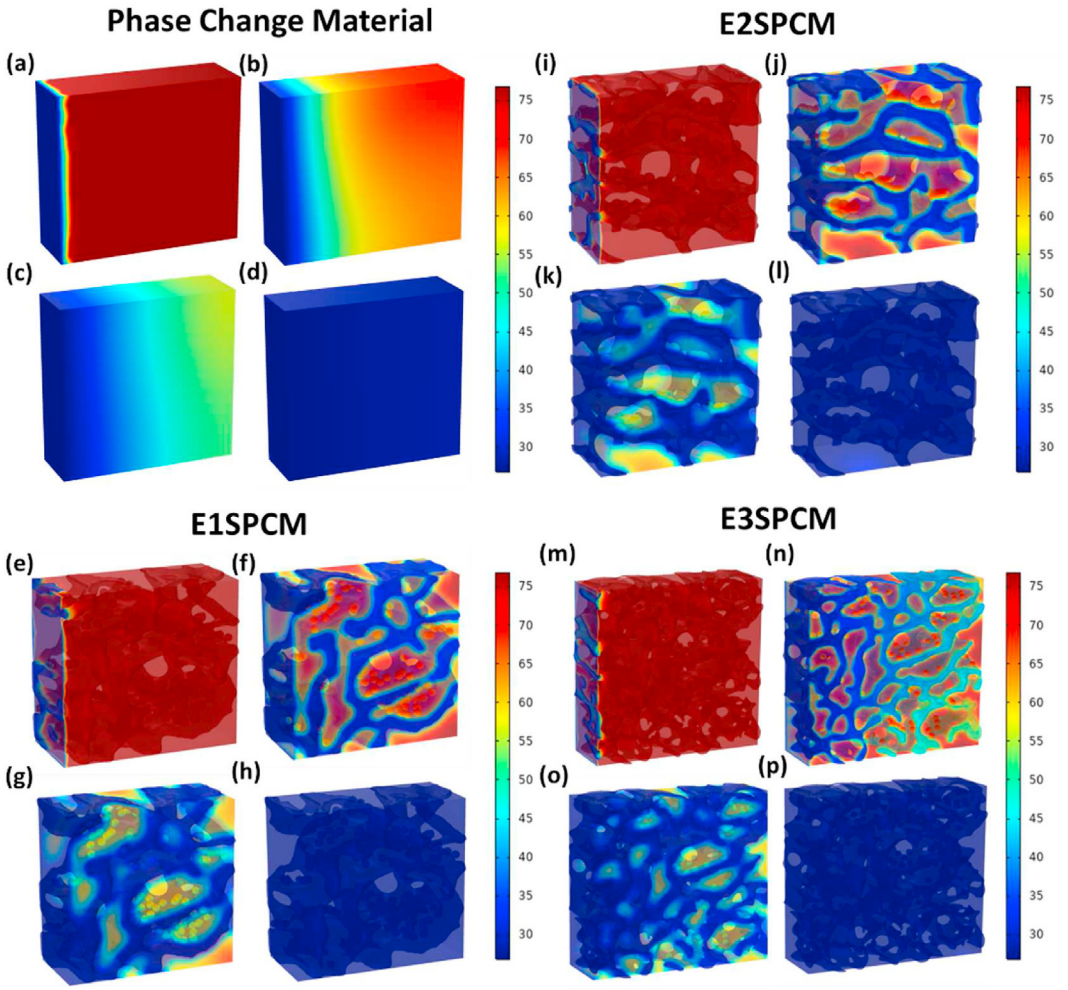

Fig. 6. COMSOL simulation of (a–d) n-hexacosane and ESPCM composite with various EG content (e–h) 5 wt% (i–l) 10 wt% and (m–p) 20 wt% respectively during solidification process.

Table 2
Reduction of time during melting and solidification process for ESPCM.

S.No	Sample	% Reduction in time during melting process	% Reduction in time during solidification process
1.	**n-hexacosane**	–	–
2.	**E1SPCM**	32.8%	22.5%
3.	**E2SPCM**	45.6%	40.2%
4.	**E3SPCM**	56.8%	52.3%

nanocomposite with different concentrations of encapsulation during the heat release process (solidification cycle) when the nanocomposite releases stored energy to the carrying media as represented in Fig. 9 (b). Subsequently, measurement of heat flow was carried out for 300 cycles of heating and cooling, and it was observed that the material shows profound stability even after repeated heat absorption and release processes which makes the nanocomposite a promising material for thermal storage applications (Fig. 9(c–d)). In addition, these results indicate that the ESPCMs have good thermal-cycle reliability as compared to pure n-hexacosane.

Fig. 10 shows the thermal stability curves of the as-prepared ESPCM composites measured using thermal gravimetric analysis (TGA). The boiling point of pure PCM is around 340–360 °C, and flashpoint between 200°C and 250 °C in air, hence the thermal stability of ESPCM was investigated within these temperature ranges. The as-prepared silica nanoparticles and exfoliated graphite nanosheets showed minor dehydration at a higher temperature, as high as 600 °C, resulting in 5% weight loss for silica and ~2% for exfoliated graphite. This result indicates exfoliated graphite and silica to be excellent encapsulation materials as both the materials showed limited loss at higher temperatures. The PCM material i.e., n-hexacosane, showed less than 2% weight loss below 200 °C, whereas maximum weight loss was observed near the boiling temperature of phase change material. The ESPCM showed nearly 3% weight loss below 200 °C with around 55% residual weight at the boiling point of 350 °C. The peak temperatures for thermal decomposition of ESPCM composites (5 wt%, 10 wt% and 20 wt%) were 184.2 °C, 190.6 °C, and 199.6 °C, respectively. The residual weights of ESPCM at the boiling point of 370 °C were observed as

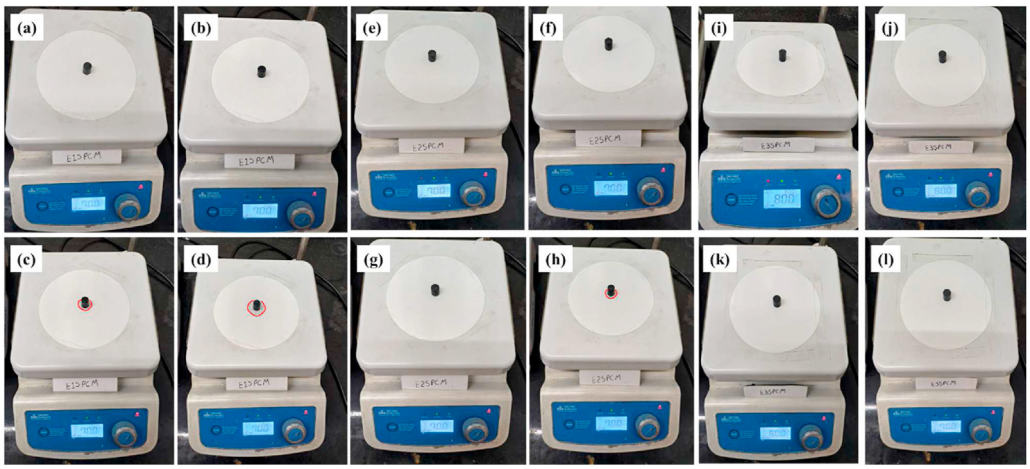

Fig. 7. Exudation-circle test diagram of various ESPCM samples with during melting process.

Table 3
Seepage-stability assessment of ESPCM composite.

Level of exudation	Avg. Circle diameter (exudation Ψ)	Leakage (%)	Range of Ψ (%)	Stability
E1SPCM	12.3	23.5	**$15 < \Psi \leq 30$**	Stable
E2SPCM	11.9	18.5	**$15 < \Psi \leq 30$**	Stable
E3SPCM	10.2	2.5	**$\Psi < 10$**	Ultra-Stable

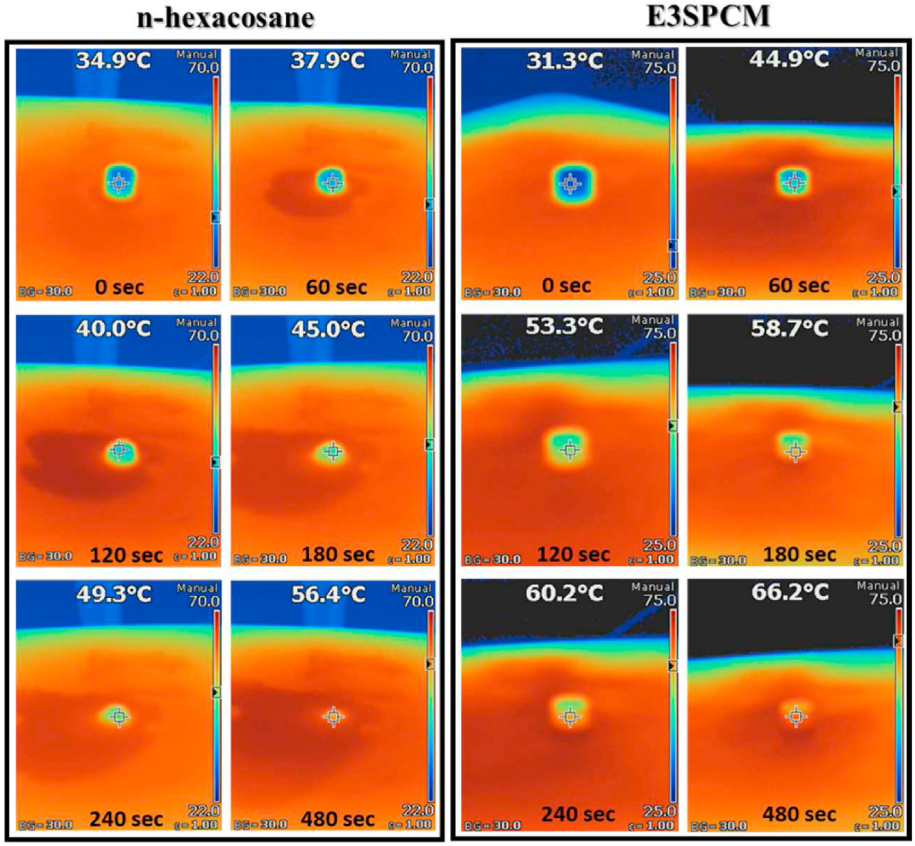

Fig. 8. IR imaging of (a) pure n-hexacosane and (b) E3SPCM.

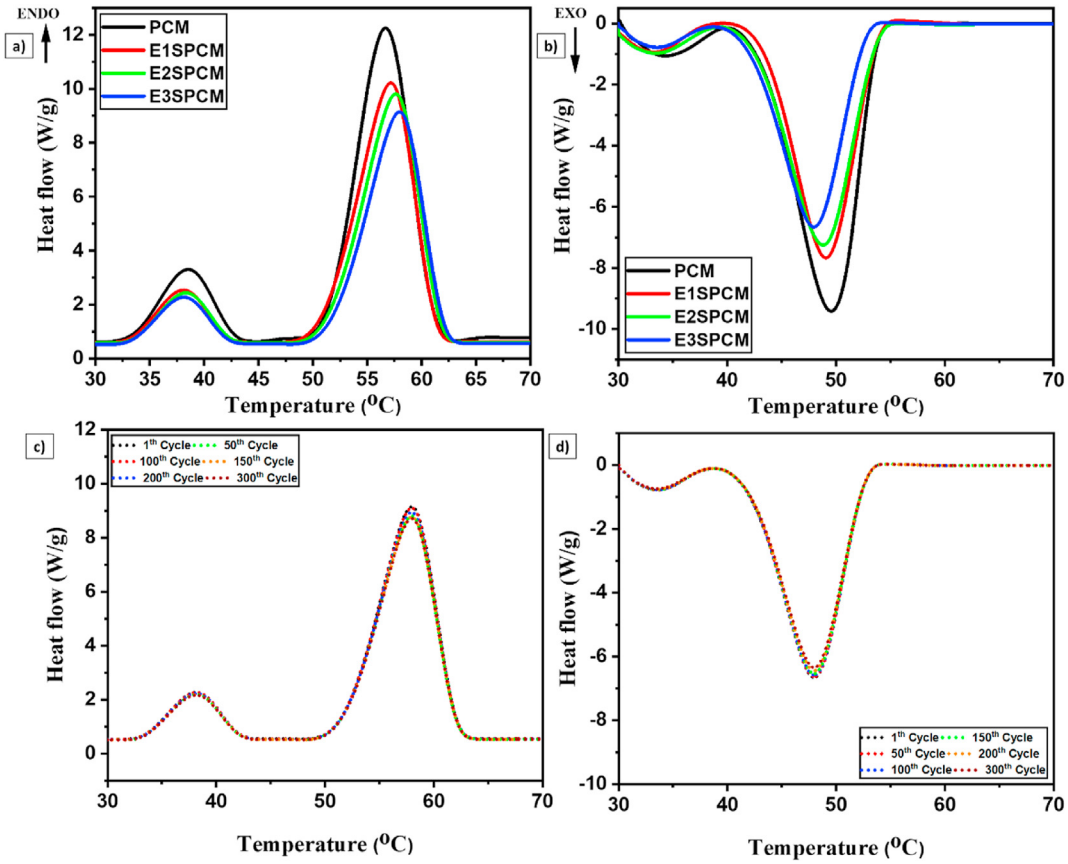

Fig. 9. (a) Melting and (b) Solidification DSC curves of the pure n-hexacosane and different ESPCM composite (c)–(d) stability of ESPCM for 300 thermal cycles.

Table 4
Experimental values during melting process of as-prepared ESPCM composites.

Samples	Phase Transition Melting Temperature (°C)	1st Cycle ΔH (J/g)	Phase Transition Solidification Temperature (°C)	1st Cycle ΔH (J/g)
n-hexacosane	54.6	184.6	49.9	176.5
E1SPCM	56.1	158.7	49.1	149.5
E2SPCM	57.6	142.8	48.8	132.7
E3SPCM	57.9	126.8	48.1	117.6

53.4%, 48.8%, and 46.4% for E3SPCM, E2SPCM and E1SPCM respectively. Also, a shift in the onset temperature for the weight loss was observed for ESPCM composites, which was higher than for n-hexacosane. The temperature at which maximum weight loss was observed for the composite was approximately 26 °C higher than for pure PCM, which reveals that the encapsulation by silica and graphitic sheets improves the thermal stability of phase change material at higher temperatures by developing a protective layer. In addition, the synthesized ultra-stable ESPCM can be used in various industrial fields such as photovoltaic, thermal and electrical storage systems [48,49].

3.7. Thermal conductivity measurements of ESPCM composites

The graphitic nanosheets not only demonstrate strong capillary forces to SPCM composites, but also have better thermal conductivity than other phase change materials [24,36]. The enhancement in thermal conductivity of the ESPCM composite largely depends on the presence of graphitic content in the composite. Fig. 11(a) shows the measured thermal conductivities of the ESPCM composites measured in relation to the latent heat storage. The result indicates that, increasing the mass fraction of EG in the composite, the overall thermal conductivity of the composite increases. The thermal conductivity of the ESPCM composites reduces after the 300th thermal cycle. A significant reduction in the thermal conductivity was observed for lower EG content (5 wt % and 10 wt %) as compared to high portions of EG (20 wt %) nanosheets after 300 cycles. This can be attributed to reduction in the composite's stability after extensive thermal cycling. It was observed that the reduced thermal conductivities of the as-prepared ESPCM composites after 300 thermal cycles were still much higher than pure PCM. The thermal conductivities of ESPCM with various EG content (5 wt %, 10 wt % and 20 wt %) were found to be 3.6 W/m K, 8.7 W/m K, 15.7 W/m K, which were 14.1, 33.6 and 60.6 times higher than pure PCM (0.26 W/m K), whereas, after 300 thermal cycles, the thermal conductivities of the ESPCM composites were obtained as 3.2 W/m K, 7.9 W/m K and 14.5 W/m K for 5 wt%, 10 wt% and 20 wt% of EG content respectively (Fig. 11(b)). For long-term operation, the thermal conductivity of the composite is determined by the compatibility of n-hexacosane encapsulated silica and exfoliated graphite nanosheets after numerous cycles, interfacial resistance and the morphology of porous dendritic structure of EG nanosheets

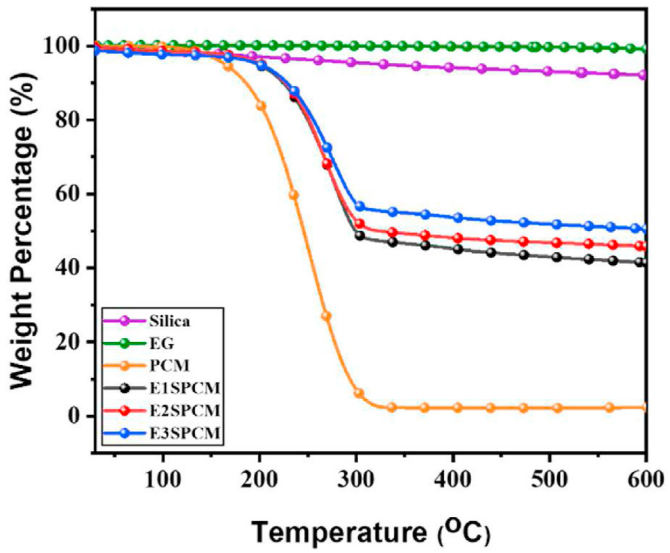

Fig. 10. TGA curve of pure n-hexcosane, expanded graphite, silica and various ESPCM composites.

in the samples, which were found well in agreement with the previous studies [42].

3.8. Thermal heat storage and release measurement

The T-history method determined the thermal heat storage and released measurement of the as-prepared ESPCM composites, as illustrated in Fig. 12(a). The details about the set-up and functioning have been discussed in section 3.2. The temperature-time curves of various ESPCM composites during the heat storage and release processes are shown in Fig. 12(a–b). The thermal storage process can be divided into different stages. It was observed that during the first stage no phase change occurs from room temperature to 54 °C and rise linearly with time for pure n-hexacosane, whereas the same rise in temperature for ESPCM composite was observed for small duration. Next, the second stage occurs between 56 °C and 74 °C, where the phase change of the materials (n-hexacosane) takes place, and the composite is filled with the melted n-hexacosane (11 min). The total time required for heat storage composites in these tests when the temperature rises from 30 °C to 74 °C were 7.8 min, 7 min, and 6.5 min for composites with E1SPCM, E2SPCM and E3PCM, respectively as shown in Fig. 9 (b) and (c).

3.9. Thermal storage system

The ultra-stable nanocomposite was studied for an application example of thermal heat storage system to understand behaviour during melting and solidification cycle. The idea was to analyse variation in the concentration of carbonaceous material (EG) with encapsulated PCM on the heat transfer between fluid and nanocomposite. Initially, a simulation study was performed using a cylindrical tank filled with as prepared phase change material having water at 70 °C as a heat source fluid as shown in Fig. S7.

Simulations were performed for melting and solidification cycles of n-hexacosane and ESPCM with respect to time as shown in Fig. 13. As represented in the figure, ES3PCM absorbs the energy from the water at higher rate compared to n-hexacosane and other samples. Complete melting of ES3PCM is observed much earlier than n-hexacosane with 40% reduction in time during melting cycle. This significant reduction in time during the melting process can be attributed to higher heat transfer rate resulted due to impregnation of expanded graphite in phase change material. During solidification cycle, water at room temperature was circulated to absorb the stored energy from the phase change material. For n-hexacosane, it was observed that water takes up the energy at slower rate as compared to ES3PCM. Heat transfer between the water and ES3PCM was efficient as compared to n-hexacosane and all the stored energy was absorbed by the water with 36% reduction in time. It was observed that impregnation resulted in substantial reduction in melting and solidification time during the heat transfer between the working fluid and nanocomposite and can serve an efficient method to store and retrieve thermal energy for engineering applications. Results of the simulation study for all the samples of ESPCM is provided in supplementary data.

To validate the results of simulation, experimental setup was developed by using a cylindrical tank having 5 tubes inside the tank for fluid circulation as shown in Fig. 14 (a). For the study, solar concentrating collector was used to maintain the temperature of water at 70 °C flowing with the rate of 40 LPH and circulated through inserted pipes [50–52]. Circulated flow of water is evenly distributed among the 5 pipes arranged in the cylindrical tank which helps in efficient heat transfer, storage, and retrieval of energy in the ESPCM during the melting and solidification cycle. During the study, parameter such as temperature and time were selected to estimate the performance of the energy storage system. The time taken to maintain the water temperature is defined with respect to heat exchange with ESPCM and the increase in PCM temperature. The phase change material system store energy in the form of latent and sensible heat. Well-designed and effective phase

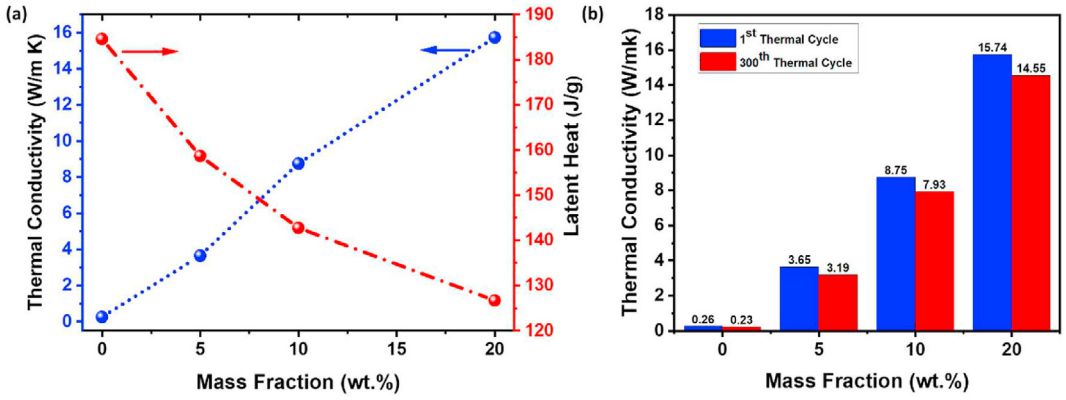

Fig. 11. (a) Relation between thermal conductivity and latent heat with various EG mass fraction of ESPCM composite. (b) Reduction in thermal conductivity after 300th thermal cycling.

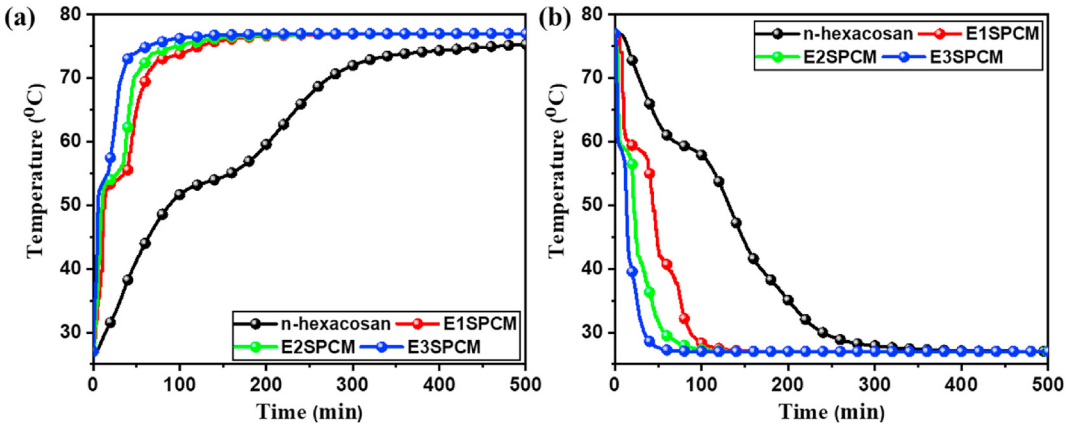

Fig. 12. Heat storage and release processes of ESPCM composites before and after thermal cycling: (a) heat storage; (b) heat release.

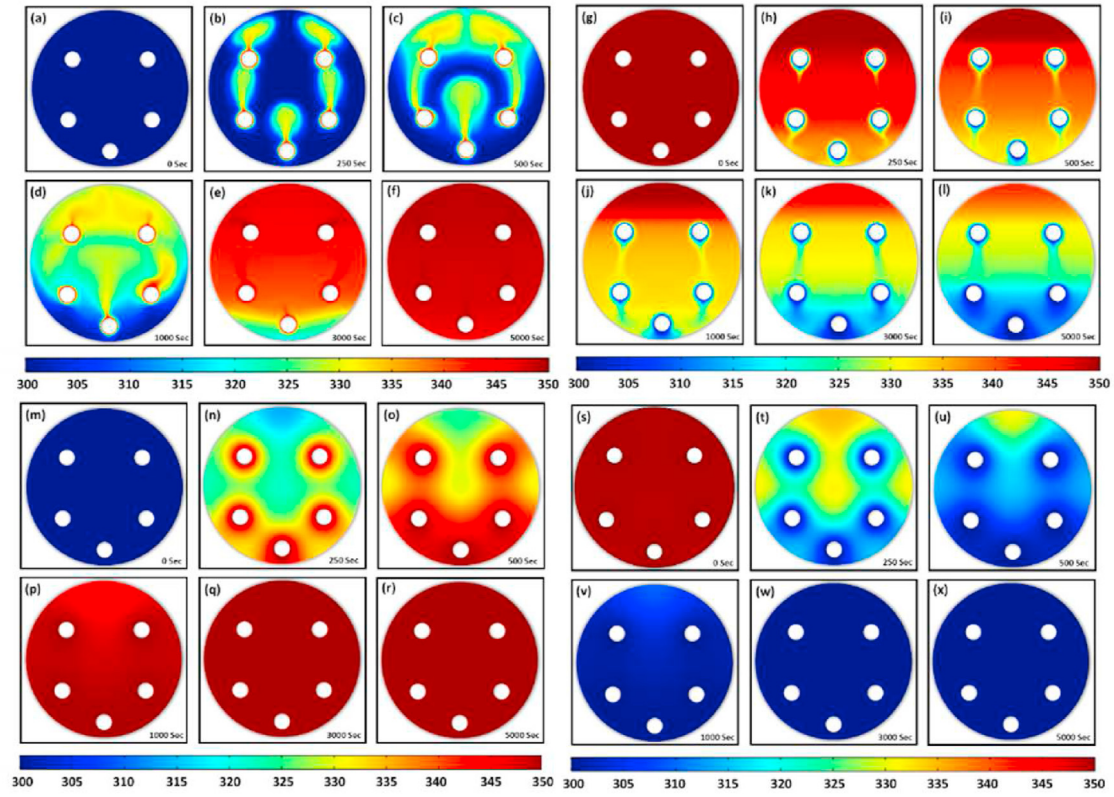

Fig. 13. COMSOL simulation of (a–l) pure n-hexacosane and (m–x) E3SPCM in the storage tank.

change material storage system takes a small charging time and confines the solid-liquid phase change within silica and expanded graphite. During the charging process, the sensible heat (H_S), latent heat (H_{LH}), latent heat of fusion (H_F) (J/kg), and overall heat stored (E_T) in the PCM storage is obtained by the equations:

$$E_s = mC_p(T - T_i) \tag{3}$$

$$E_{LH} = mH_f\theta \tag{4}$$

$$E_T = mC_p(T - T_i) + mH_f\theta = E_s + E_{LH} \tag{5}$$

Initially, the ESPCM unit stores sensible heat. Because of the high-temperature difference between the inlet water and solid ESPCM, the rate of sensible heat storage is more than the latent heat storage system. Once the temperature of ESPCM reaches close to its transition temperature, the system starts storing latent heat, which is released later, making the heat management mechanism efficient. The experimental results obtained were found in agreement with the simulated results, as shown in Fig. 14 (b and c). Thus, making the synthesized material as a promising material for commercialization or industrial application.

4. Conclusion

In this work, we demonstrated a simple, versatile, and scalable chemical process to prepare encapsulated n-hexacosane silica composites loaded within exfoliated graphite (ESPCM) for thermal

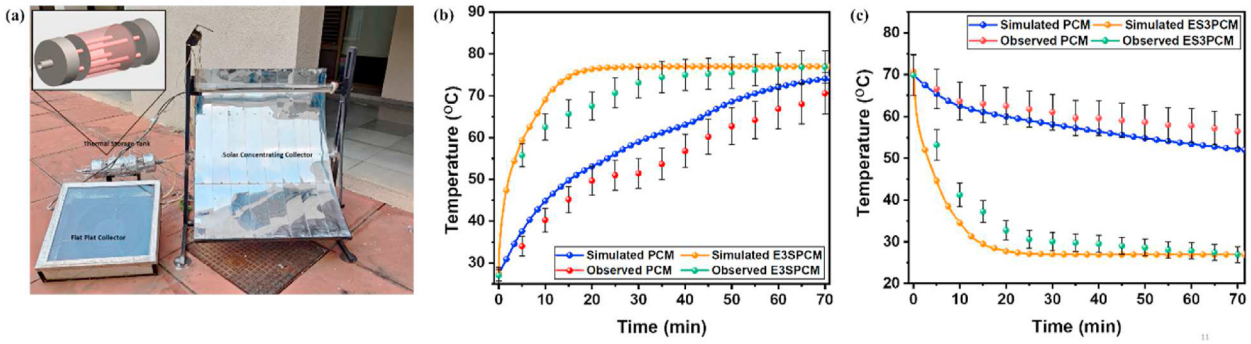

Fig. 14. Heat storage system to measure thermal change, (a) experimental set-up, Graph showing the measured and simulated thermal change (b) melting, and (c) solidification cycle.

storage systems. The morphological and structural analysis confirms the formation of the ESPCM composite with no chemical reaction between the materials. The exfoliated graphite acts as the supporting material which improves the thermal conductivity, stability of the composites and helps in preventing any leakages even when the core material is heated above its melting temperature. The ultra-stable ESPCM composite maintains its phase transition perfectly and helps the composite to melt at 57.9 °C with a latent heat of 127 J/g and solidify at 48.1 °C with a latent heat of 118 J/g. Adding exfoliated graphite and silica to phase change materials not only enhanced the thermal conductivity but stabilized the composite and addressed the leakage issue of PCMs during their liquid state. Also, the COMSOL simulation of the pure PCM and nanocomposites was carried out, which was found to support the experimental results. Thus, the fabricated ESPCM can work as an excellent thermal storage material for industrial applications.

Declaration of competing interest

The authors declare that they have no known competing financial interests or personal relationships that could have appeared to influence the work reported in this paper.

Acknowledgement

The authors would like to thank CSIR - Council of Scientific & Industrial Research (09/1074(0004/2018 EMR-I), and Pandit Deendayal Energy University, PDPU for providing the necessary facilities to carry out this investigation. Authors are thankful for the collaboration and support from Heat Pipe and Thermal Management Research Group, Brunel University London, UK.

Appendix A. Supplementary data

Supplementary data to this article can be found online at https://doi.org/10.1016/j.energy.2022.123729.

References

[1] Jouhara H, Olabi AG. Industrial waste heat recovery. Energy 2018;160:1–2.
[2] Prajapati Pp PP, Patel VK. Comparative analysis of nanofluid-based Organic Rankine Cycle through thermoeconomic optimization. Heat Tran Asian Res 2019;48(7):3013–38.
[3] Olabi AG, Abdelkareem MA. Energy storage systems towards 2050. Energy 2021;15. 219:119634.
[4] Prajapati Pp PP, Patel VK. Thermo-economic optimization of a nanofluid based organic Rankine cycle: a multi-objective study and analysis. Therm Sci Eng Prog 2020;17:100381. 1.
[5] Olabi AG, Onumaegbu C, Wilberforce T, Ramadan M, Abdelkareem MA, Al–Alami AH. Critical review of energy storage systems. Energy 2021;214:118987.
[6] Ahmad L, Khordehgah N, Malinauskaite J, Jouhara H. Recent advances and applications of solar photovoltaics and thermal technologies. Energy 2020;207:118254.
[7] Righetti G, Doretti L, Zilio C, Longo GA, Mancin S. Experimental investigation of phase change of medium/high temperature paraffin wax embedded in 3D periodic structure. Int J Thermofluids 2020;5:100035.
[8] Okogeri O, Stathopoulos VN. What about greener phase change materials? A review on biobased phase change materials for thermal energy storage applications. Int J Thermofluids 2021;10:100081. May 1.
[9] Amini A, Miller J, Jouhara H. An investigation into the use of the heat pipe technology in thermal energy storage heat exchangers. Energy 2017;136:163–72.
[10] Jouhara H, Żabnieńska AG, Khordehgah N, Ahmad D, Lipinski T. Latent thermal energy storage technologies and applications: a review. Int J Thermofluids 2020;1:100039.
[11] Paneliya S, Khanna S, Patel U, Prajapati P, Mukhopadhyay I. Systematic investigation on fluid flow and heat transfer characteristic of a tube equipped with variable pitch twisted tape. Int J Thermofluids 2020;1:100005.
[12] Paneliya S, Khanna S, Prajapati P, Borad A. Computational analysis of copper@paraffin composite in a cylindrical cavity for enhanced thermal energy storage system. Mater Today Proc 2021;43:541–6.
[13] Ajji Z, Jouhara H. Investigation of the effects of thermal, oxidative and irradiation treatments on the behaviour of poly-ethylene glycol as a phase change material in thermal energy storage systems. Energy 2017;136:196–200.
[14] Singh AP, Khanna S, Paneliya S, Hinsu H, Patel Y, Mehta B. Preparation and characterization of solid-state neopentyl glycol/expanded graphite micro composite for thermal energy storage applications. Mater Today: Proceedings 2020;47(105):621–5. https://doi.org/10.1016/j.matpr.2020.11.403.
[15] Giro-Paloma J, Martínez M, Cabeza LF, Fernández AI. Types, methods, techniques, and applications for microencapsulated phase change materials (MPCM): a review. Renew Sustain Energy Rev 2016;53:1059–75.
[16] Zhang XX, Fan YF, Tao XM. Fabrication and properties of microcapsules and nanocapsules containing n-octadecane. Mater Chem Phys 2004;88:300–7.
[17] Ahmet Sarı, Cemil Alkan, Ali Karaipekli. Preparation characterization and thermal properties of PMMA/n-heptadecane microcapsules as novel solid–liquid microPCM for thermal energy storage. Appl Energy 2010;87:529–34.
[18] Zhou XF, Xiao HN, et al. Preparation and thermal properties of paraffin/porous silica ceramic composite. Compos Sci Technol 2009;69:1246–9.
[19] Qiang Z, Luo Z, Guo Q, Wu G. Preparation and thermal properties of short carbon fibers/erythritol phase change materials. Energy Convers Manag 2017;136:220–8.
[20] Zuo X, Zhao X, Li J, Hu Y, Yang H, Chen D. Enhanced thermal conductivity of form-stable composite phase-change materials with graphite hybridizing expanded perlite/paraffin. Sol Energy 2020;209:85–95.
[21] Sivasankaran H, Ishikawa K, Einarsson E, Aikawa S, Inoue T, Zhao P, Watanabe M, Chiashi S, Shiomi J, Maruyama S. Temperature dependent thermal conductivity increase of aqueous nanofluid with single walled carbon nanotube inclusion. Mater Express 2012;2:213–23.
[22] Zhang Z, Liu Y, Wang J, Sun L, Xie T, Yang K, Li Z. Preparation and characterization of high efficiency microencapsulated phase change material based on paraffin wax core and SiO2 shell derived from sodium silicate precursor. Colloids Surf A Physicochem Eng Asp 2021;26:126905.
[23] Li M, Wu Z, Tan J. Properties of form-stable paraffin/silicon dioxide/expanded graphite phase change composites prepared by sol-gel method. Appl Energy 2012;92:456–61.
[24] Xu T, Chen Q, Huang G, Zhang Z, Gao X, Lu S. Preparation and thermal energy storage properties of d-Mannitol/expanded graphite composite phase change material. Sol Energy Mater Sol Cell 2016;155:141–6.
[25] Karaipekli A, Sarı A, Kaygusuz K. Thermal conductivity improvement of stearic acid using expanded graphite and carbon fiber for energy storage applications. Renew Energy 2007;32(13):2201–10.
[26] Fang G, Li H, Chen Z, Liu X. Preparation and characterization of stearic acid/expanded graphite composites as thermal energy storage materials. Energy

2010;35(12):4622–6.
[27] Zhang H, Gao X, Chen C, Xu T, Fang Y, Zhang Z. A capric–palmitic–stearic acid ternary eutectic mixture/expanded graphite composite phase change material for thermal energy storage. Compos Appl Sci Manuf 2016;87:138–45.
[28] Yang X, Yuan Y, Zhang N, Cao X, Liu C. Preparation and properties of myristic–palmitic–stearic acid/expanded graphite composites as phase change materials for energy storage. Sol Energy 2014;99:259–66.
[29] Wen R, Zhang X, Huang Y, Yin Z, Huang Z, Fang M, Liu Yg, Wu X. Preparation and properties of fatty acid eutectics/expanded perlite and expanded vermiculite shape-stabilized materials for thermal energy storage in buildings. Energy Build 2017;139:197–204.
[30] Hu P, Yu J-J, Wang X-W. Preparation and thermal performance of palmitic acid/expanded graphite composite phase change materials. J Eng Thermophys 2017;38:464–9.
[31] Zhou D, Yuan J, Zhou Y, Liu Y. Preparation and characterization of myristic acid/expanded graphite composite phase change materials for thermal energy storage. Sci Rep 2020;10(1):1–11.
[32] Atinafu DG, Wi S, Yun BY, Kim S. Engineering biochar with multiwalled carbon nanotube for efficient phase change material encapsulation and thermal energy storage. Energy 2021;216:119294.
[33] Paneliya S, Khanna S, Singh AP, Patel YK, Vanpariya A, Makani NH, Banerjee R, Mukhopadhyay I. Core shell paraffin/silica nanocomposite: a promising phase change material for thermal energy storage. Renew Energy 2021;167:591–9.
[34] Khanna S, Utsav, Marathey P, Chaliyawala H, Rajaram N, Roy D, Banerjee R, Mukhopadhyay I. Fabrication of long-ranged close-packed monolayer of silica nanospheres by spin coating. Colloid Surface Physicochem Eng Aspect 2018;553:520–7.
[35] Utsav S Khanna, Paneliya S, Ray A, Mukhopadhyay I, Banerjee R. Controlled etching of silica nanospheres monolayer for template application: a systematic study. Appl Surf Sci 2020;500:144050.
[36] Khanna S, Utsav, Chaliyawala H, Paneliya S, Roy D, Mukhopadhyay K, Banerjee R, Mukhopadhyay I. Systematic investigation of close-packed silica nanospheres monolayer under sintering conditions. J Eur Ceram Soc 2019;39:1411–9.
[37] Khanna S, Marathey P, Paneliya S, Vanpariya A, Ray A, Banerjee R, Mukhopadhyay I. Fabrication of silicon nanohorns via soft lithography technique for photoelectrochemical application. Int J Hydrogen Energy 2021;46:16404–13.
[38] Khanna S, Paneliya S, Marathey P, Shah K, Prajapati P, Chaudhari R, Vora J. Investigation of thermophysical properties of synthesized N-Hexacosane-Encapsulated titania phase change material for enhanced thermal storage application. Recent Adv Mech Infrast 2022:107–18 [Springer, Singapore].
[39] Utsav S Khanna, Mukhopadhayay I, Banerjee R. Self-assembly of silica nanoparticles by tuning substrate-adsorbate interaction. In: AIP conference proceedings. AIP Publishing LLC; 2018, 030001.
[40] Utsav, Khanna S, Paneliya S, Makani NH, Mukhopadhyay I, Banerjee R. Controlled restructuring of bidisperse silica nanospheres for size-selective nanowire growth. Mater Chem Phys 2021;15:125063.
[41] Pandey U, Khanna S, Paneliya S, Makani NH, Mukhopadhyay I, Banerjee R. Thermal crowning mechanism in gold-silica nanocomposites: plasmonic-photonic pairing in archetypal two-dimensional structures. Phys Chem Chem Phys 2021;23:17197–207.
[42] Khanna S S, Marathey P, Utsav, Chaliawala H, Mukhopadhyay I. Bidisperse silica nanoparticles close-packed monolayer on silicon substrate by three step spin method. In: AIP conference proceedings 1961; 2018, 030042.
[43] Wu Y, Wang T. Hydrated salts/expanded graphite composite with high thermal conductivity as a shape-stabilized phase change material for thermal energy storage. Energy Convers Manag 2015;101:164–71.
[44] Krupa I, Nógellová Z, Špitalský Z, Malíková M, Sobolčiak P, Abdelrazeq HW, Ouederni M, Karkri M, Janigová I, Al-Maadeed MAS. Positive influence of expanded graphite on the physical behavior of phase change materials based on linear low-density polyethylene and paraffin wax. Thermochim Acta 2015;614:218–25.
[45] Mochane M, Luyt A. The effect of expanded graphite on the flammability and thermal conductivity properties of phase change material based on PP/wax blends. Polym Bull 2015;72(9):2263–83.
[46] Al Maadeed M, Labidi S, Krupa I, Karkri M. Effect of expanded graphite on the phase change materials of high-density polyethylene/wax blends. Thermochim Acta 2015;600:35–44.
[47] Paneliya S, Khanna S, Utsav, Makani NH, Banerjee R, Mukhopadhyay I. Highly stable n-hexacosane loaded exfoliated graphite nanosheets for enhanced thermal energy storage application. J Energy Storage 2022;48:103903. https://doi.org/10.1016/j.est.2021. 103903.
[48] Rashad M, Khordehgah N, Żabnieńska AG, Ahmad L, Jouhara H. The utilisation of useful ambient energy in residential dwellings to improve thermal comfort and reduce energy consumption. Int J Thermofluids 2021;1:100059.
[49] Khordehgah N, Żabnieńska AG, Jouhara H. Analytical modelling of a photovoltaics-thermal technology combined with thermal and electrical storage systems. Renew Energy 2021;165:350–8.
[50] Paneliya S, Khanna S, Prajapati P, Borad A. Computational analysis of copper@paraffin composite in a cylindrical cavity for enhanced thermal energy storage system. Mater Today Proc 2021;43:541–6.
[51] S. Paneliya, P. Prajapati P, U. Patel, I. Trivedi, A. Patel, K. Patel, S. Khanna, Experimental and CFD analysis on heat transfer and fluid flow characteristic of a tube equipped with variable pitch twisted tape, E3S web of conferences 2019 (Vol. vol. 116, p. 00058). EDP Sciences.
[52] Paneliya S, Khanna S, Mehta J, Kathiriya V, Patel U, Prajapati P, Mukhopdhyay I. An experimental and CFD analysis on heat transfer and fluid flow characteristics of a tube equipped with X-shaped tape insert in a U-shaped heat exchanger. In: Proceedings of the 7th international conference on advances in energy Research. Singapore: Springer; 2021. p. 1331–48.